SERI/TP-211-3667
DE90000320

March 1990

Research on Amorphous Silicon-Based Thin Film Photovoltaic Devices Task B: Research on Stable High Efficiency Large Area, Amorphous Silicon-Based Submodules

Semi-Annual Subcontract Report 16 March 1989 - 30 November 1989

A. E. Delahoy, F. B. Ellis, C. Kothandaraman, H. Schade, T. Tonon, H. Weakliem
Chronar Corporation
Princeton, New Jersey

Prepared under Subcontract No. ZB-7-06003-1

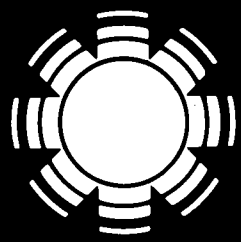

SERI

Solar Energy Research Institute
A Division of Midwest Research Institute
1617 Cole Boulevard
Golden, Colorado 80401

Operated for the
U.S. Department of Energy
under Contract No. DE-AC02-83CH10093

This publication was reproduced from the best available camera-ready copy submitted by the subcontractor and received no editorial review at SERI.

NOTICE

Printed in the United States of America
Available from:
National Technical Information Service
U.S. Department of Commerce
5285 Port Royal Road
Springfield, VA 22161

Price: Microfiche A01
Printed Copy A03

Codes are used for pricing all publications. The code is determined by the number of pages in the publication. Information pertaining to the pricing codes can be found in the current issue of the following publications which are generally available in most libraries: *Energy Research Abstracts (ERA)*; *Government Reports Announcements* and Index (*GRA* and I); *Scientific and Technical Abstract Reports (STAR)*; and publication NTIS-PR-360 available from NTIS at the above address.

SERI/TP-211-3667
UC Category: 271
DE90000320

SERI/TP--211-3667

DE90 000320

Research on Amorphous Silicon-Based Thin Film Photovoltaic Devices
Task B: Research on Stable High-Efficiency Large Area, Amorphous Silicon-Based Submodules

Semi-Annual Subcontract Report
16 March 1989 - 30 November 1989

A. E. Delahoy
F. B. Ellis
C. Kothandaraman
H. Schade
T. Tonon
H. Weakliem
Chronar Corporation
Princeton, New Jersey

March 1990

SERI Technical Monitor: W. Luft

Prepared under Subcontract No. ZB-7-06003-1

Solar Energy Research Institute
A Division of Midwest Research Institute

1617 Cole Boulevard
Golden, Colorado 80401-3393

Prepared for the
U.S. Department of Energy
Contract No. DE-AC02-83CH10093

PREFACE

This Semi-Annual Report covers research performed by Chronar Corporation during the period March 16, 1989 to November 30, 1989, under subcontract No. ZB-7-06003-1. This period represents the first half of Phase III of a 3-year, cost-shared program. The program manager is Dr. Alan E. Delahoy. The contributors to research reported here are listed below:

Mr. J.A. Cambridge	
Mr. H. Chao	
Dr. A.E. Delahoy	Principal Investigator Subtask B1/B2
Dr. F.B. Ellis, Jr.	
Dr. E. Eser	
Mr. H. Field	
Dr. S.C. Gau	
Mr. J. Houghton	
Mr. J. Kalina	
Dr. F.J. Kampas	Principal Investigator Subtask B3
Mr. C. Kothandaraman	
Mr. L. Michalski	
Mr. R. Radeztsky	
Mr. F. Ramos	
Mr. A. Savary	
Dr. H. Schade	
Mr. W. Stroud	
Dr. T. Tonon	
Dr. H.A. Weakliem	

Delays in some areas of research were encountered during this time period owing to the relocation of Chronar's research laboratories to the Headquarters building at 195 Clarksville Road, Lawrenceville, NJ 08648.

TABLE OF CONTENTS

List of Figures

List of Tables

SUMMARY

Objective

The primary objective of this subcontract is to develop amorphous silicon p-i-n/p-i-n tandem junction photovoltaic submodules (> 900 cm^2) having an aperture area efficiency of at least 9%. A further objective is to demonstrate 8% tandem submodules that degrade by no more than 5% under standard light soaking conditions.

Discussion

The main lines of investigation during this period concerned the exploration of novel types of p-layers, the properties and applications of doped zinc oxide films to a-Si:H cells, the effects of various surface treatments of SnO_2 and ZnO transparent conducting oxides (TCO's) on cell performance, the dependence of cell stability on substrate and junction type, and the development of techniques to enable the full potential performance of the a-Si:H to be realized in a module configuration.

The novel p-layers included p-layers consisting of two sublayers. The first deposited sublayer consisted of a conventional, but thin $a\text{-}Si_{1-x}C_x$:H layer, while the second consisted either of a similar layer prepared using high hydrogen dilution, or a non-carbon containing layer prepared under microcrystalline conditions. The $(a\text{-}SiC)_1/(a\text{-}SiC)_2$ approach appeared capable of higher efficiencies.

We consider it important and potentially instructive to compare the use of an alternative transparent conductor to SnO_2, and have selected ZnO for this purpose. High quality Al-doped ZnO films were prepared by magnetron sputtering, and the properties of cells prepared on SnO_2, and SnO_2 overcoated with ZnO, were compared. It was found that standard deposition procedures developed for SnO_2 lead to cells on SnO_2-ZnO with poor fill factors, but that pre-deposition treatment of the ZnO in an oxygen-containing plasma lowers the ZnO/p-layer contact resistance, thereby enabling efficient cells to be fabricated. Higher open-circuit voltages were consistently observed on ZnO compared with those on SnO_2.

Work on the application of ZnO to a back reflector/back contact was continued, and an external quantum efficiency of 46% was obtained at 700 nm with a ZnO/$BaSO_4$ reflector. Further physical, electrical and optical characterization of sputtered ZnO:Al films was pursued, using techniques such as Auger analysis, EDX, SEM, 4-point probe, Hall effect, X-ray diffraction, and spectrophotometry.

The comparative photostability of various cell types was determined in a large light soaking study. One of the most remarkable outcomes of this study was the observation that single junction cells prepared on a SnO_2 substrate overcoated with ZnO in one particular a-Si:H run outperformed all other single junction cells prepared on bare SnO_2. Indeed, the stabilized efficiency of these single junction cells on ZnO (6.3%) exceeded the stabilized efficiency of all but one group of tandem junction cells on SnO_2.

Preliminary results have been obtained which indicate that it is possible to improve the photostability of a-Si:H cells via a post-deposition treatment. The treatment involves high intensity irradiation at 170°C followed by an extended anneal at that temperature.

In the area of submodules a laser/etch technique was developed that guaranteed good cell-cell isolation, thereby improving the yield of the laser Al isolation process. Progress was also made towards developing a technique for the simultaneous removal of shunt-type defects over large areas. In the patterning area, reasonably low interconnect resistances were obtained via a laser fusing technique which would obviate the need to laser scribe the a-Si:H.

Long term outdoor exposure tests of glass-glass encapsulated tandem submodules have indicated an 11% power loss over a period of 145 days, a quite acceptable result.

Conclusions

- The importance of TCO surface treatment has been demonstrated. In particular, it was found that treatment of ZnO in an oxygen-containing plasma is necessary for the attainment of high quality cells on ZnO.
- Higher open-circuit voltages have been consistently obtained on ZnO compared to the standard SnO_2 substrate.
- Single junction cells having a record 6.3% stabilized efficiency were prepared on SnO_2 overcoated with ZnO.
- A laser/etch technique was developed that guarantees good cell-cell isolation in submodules.
- Progress has been made on a laser-fusing technique for forming the cell interconnects, and on a method of large area defect removal.

SECTION 1.0

INTRODUCTION

This research program is designed to advance the state-of-the-art in a-Si:H photovoltaic submodule performance. The research encompasses both single and tandem junction submodules in 1 sq.ft. or 1 x 3 sq.ft. sizes, with specific goals for efficiency and stability. From Phase II (roughly FY88) onwards, the emphasis has been, and will continue to be, placed on tandem devices because of their superior stability.

The research is divided into three fields (subtasks B1, B2, and B3), as follows:

B1. Semiconductor Materials and Small Area Cells. The objectives here include the deposition of amorphous silicon materials over large areas, the optimization of these materials as guided by physical, chemical, electrical and optical characterization, and the optimization of the efficiency and stability of small area p-i-n and p-i-n/p-i-n cells.

B2. Non-Semiconductor Materials. Here the objectives are the deposition of front and back contact materials (transparent conductors and metallization) over large areas, the development of advanced back reflectors, minimization of optical losses, and study of the thermal stability of the associated materials and interfaces.

B3. Submodules. The objectives here are the fabrication and optimization of large area interconnected devices on a monolithic substrate. This includes investigation of submodule configurations and patterning approaches, increase of active area, defect analysis, and a comparison of the light soak behavior of single and tandem junction submodules.

The main findings and results established during the first half of Phase III are described below. They are categorized according to the appropriate subtask.

2.0 SEMICONDUCTOR MATERIALS AND SMALL AREA CELLS

2.1 Optimized Semiconductor Layers

Deposition conditions for the optimized versions of the various semiconductor layers employed in the fabrication of tandem junction cells are listed in Table I. The cell structure is p_1(a-SiC)-i_{t1}(a-SiC)-i_1(a-Si) -n_1(a-Si)/p_2(a-SiC)-i_{t2}(a-SiC)-i_2(a-Si)-n_2(μc-Si), where a-SiC really denotes a-$Si_{1-x}C_x$:H, etc. Plasma cleaning and flushing cycles are included for completeness, as are the conditions for p-type microcrystalline silicon layers, and the amorphous n layer occasionally employed in single junction cells. Single junction p, i_t, i, and n layers are identical to tandem junction p_1, i_{t1},i_1 (or i_2) and n_2 layers, except regarding i-layer thickness.

Table I. Deposition sequence and conditions for tandem cells.

	Absolute flow rates in sccm									
Process	SiH_4	CH_4	H_2	B_2H_6	PH_3	Ar	He	Press. (mtorr)	RF pwr (W)	Time
1. Ar plasma						39.0		166	35	15 m
2. p_1(a-SiC)	10.0	12->7.5		0.22			7.1	300	23	34 s
3. Post p_1 pumpdwn								vac.		5 m
4. Post p_1 flush	10.0		22					130		21 m
5. i_{t1}(a-SiC)	25.0	12->0.0	56					500	19	105 s
6 i_1(a-Si)	25.0		56					500	12	
7. n_1(a-Si)	5.0		45		0.40	20.0		350	45	110 s
8. Post n_1 H plas.			48					500	8	4.5 m
9. Post n_1 flush	10.0		22					130		58 m
10. p_2(a-Si)	10.0	12->7.5		0.28			9.0	300	23	30 s
11. Post p_2 pmpdwn								vac.		5 m
12. Post p_2 flush	10.0		22					130		21 m
13. i_{t2}(a-SiC)	25.0	12->4.2*	56					500	19	233 s
14. i_2(a-Si)	25.0		56					500	12	
15. n_2(uc-Si)	1.0		95		0.014	0.70		1000	60	16 m
a. p(uc-Si)	2.5		95	0.06			1.9	500	90	
b. n(a-Si)	5.0		45		0.40	20.0		350	45	6 m

Notes:

1. All deposition temperatures are 180°C
2. a-SiC denotes a-$Si_{1-x}C_x$:H, etc.
3. Entries a.) and b.) are other standard layers not employed in tandem cells.

*4. The CH_4 flow for i_{t2} is reduced to 4.2 sccm in 53 seconds; this flow is then maintained for a further 3 minutes.

2.2 P-layer Research

As mentioned in section 2.1 above, our standard, optimized amorphous silicon carbide p-layers have been prepared under the following conditions:

temperature	180°C
pressure	300 mTorr (as measured 60 cm downstream from the vacuum chamber)
rf power	22 watts net (power density 11 mW/cm^2)
time	34 seconds
SiH_4 flow	10 sccm
CH_4	12 sccm graded to 7.5 sccm
B_2H_6 flow	0.22 sccm in 7.1 sccm He

These conditions were established largely through p-i-n device optimization. However, while fill factor (0.68-0.70) and blue response (QE of 0.7 at 400nm) have been satisfactory, open circuit voltages have tended to fall in the range 820-830 mV. This we feel can be improved without necessarily sacrificing other parameters. Bearing in mind that V_{OC} is controlled largely by the properties of the p-layer and transitional i-layer, we experimented with 4 variations of these p-layer conditions. (Of course, the p-layer can also affect J_{SC} and FF). The 4 variations and their salient conditions are listed below:

type a. a-SiC; identical parameters, except higher rf power (30-40W)

type b. a-SiC; modified gas flows, and higher rf power (30W)

type c. a-SiC/μc-Si; for μc-Si: 90W, high H_2 dilution, no CH_4

type d. $(a\text{-}SiC)_1/(a\text{-}SiC)_2$; second layer 50W with high H_2 dilution

All of these variations involve use of a higher rf power; in types a,b, and d the motivation is to open the p-layer gap (through increased incorporation of carbon) in order to increase V_{OC}, in type c the high power is associated with the intention of growing microcrystalline silicon, again to increase V_{OC}. For films of type b the gas phase diborane and methane concentrations were reduced in conjunction with the higher rf power and longer deposition time.

In type c, amorphous silicon carbide was put down before switching to microcrystalline deposition conditions, since we had shown previously that μc-Si nucleates far more readily on a-Si than on glass or SnO_2 [1]. In type d we wished to prepare a p-layer using H_2 dilution of the source gases, but to avoid excessive reduction of the SnO_2 grew thin a-SiC layers without H_2 dilution first. Examples of results obtained using these types of p-layer are contained in Table II. (This table represents a condensation of run conditions and cell performance for the various single junction cells that are referred to in this report).

In terms of the average efficiency of dot cells distributed over a 1 ft.sq. substrate, the results may be conveniently summarized as follows:

type a.	a-SiC, higher power,	run 428, 8.7% (on ZnO) run 442, 8.64% (on SnO_2)
type b.	a-SiC, higher power, reduced B_2H_6 and CH_4, longer deposition,	run 446, 8.88% (SnO_2)
type c.	a-SiC/μc-Si	run 431, 5 min μc, 8.39% (SnO_2) run 434, 1 min μc, 8.59% (SnO_2)
type d.	$(a\text{-}SiC)_1/(a\text{-}SiC)_2$	run 451, 8.58% (25W/50W, SnO_2) run 452, 8.77% (50W/50W, SnO_2)

These results may be compared to the best result obtained with the standard p-layer during this time period, namely 8.55% on SnO_2 in run 456. The incremental improvement in performance exhibited by type b and type d p-layers on SnO_2 suggests that further development of those types would be warranted. It may be noted that p-(a-SiC_A)/p-(a-SiC_B) multilayer p-layers of the form ABABA, with bandgaps of 2.2 and 1.9eV for the A and B sublayers, have been successfully used by Tanaka et al. in the preparation of a 12.0% single junction cell [2]. The J-V curve of the best small area cell produced in this series is shown in Fig. 1. The cell was prepared on glass/SnO_2, and employed a type b p-layer (run 446). The V_{oc} of this cell was 864 mV and it attained an efficiency of 9.6% with an Al back contact.

It may be noted that a high average V_{oc} of 892 mV was obtained in run 431 by employing a 5 min μc-Si p-layer in conjunction with a ZnO substrate, although we have no evidence that such a thin layer prepared under microcrystalline conditions is in fact microcrystalline.

Table II. Average dot parameters for single-junction runs.

Run #	Plate & TCO	V_{oc} (mV)	J_{sc} (mA/cm^2)	FF (%)	Eff (%)	R_s (ohm cm^2)	Comments
405	LW SnO_2	842	15.0	66.5	8.40	7.0	
	LE SnO_2-ZnO	866	15.4 ( )	53.0	7.08	21.1	
424	LW SnO_2	796	14.2	66.9	7.54	6.3	5 min O_2, 0.4 um
	LE SnO_2-ZnO	820	13.8	73.1	8.25	4.4	
	RE SnO_2-ZnO-TiO_x	804	13.6	73.9	8.08	4.3	
425	LW ZnO	870	13.2	56.7	6.51	12.4	1 min H_2, double n
	LE SnO_2-ZnO	854	14.1	67.9	8.20	5.8	
	RE SnO_2	828	14.5	71.1	8.55	5.2	
427	LW SnO_2-ZnO	834	14.7	65.8	8.07	5.8	5 min H_2/5 min O_2
	LE SnO_2-ZnO	837	15.3	66.0	8.45	5.4	
	RW ZnO	815	10.8	61.6	5.41	12.3	
428	LW SnO_2	823	15.1	65.8	8.19	6.6	3 min O_2, 30W p, double n
	LE SnO_2-ZnO	842	14.9	69.4	8.70	4.9	
431	LW SnO_2-ZnO	892	12.1	65.0	7.00	12.8	5 min O_2, 20s a/5m uc p
	RW SnO_2	830	13.7	74.0	8.39	4.4	
433	LW ZnO	812	12.4	55.3	5.59	13.1	Ts = 205°C, 3 min O_2
	LE SnO_2-ZnO	831	13.6	66.5	7.49	6.4	
	RE SnO_2	754	14.7	73.4	8.14	4.1	
434	LE SnO_2	812	15.9	66.7	8.59	4.5	34s a/1m uc p
442	LW SnO_2	814	15.8	67.2	8.64	5.3	No O_2, 40W p
	LE SnO_2-ZnO	827	14.1	66.9	7.82	8.3	
446	LW SnO_2	845	15.4	68.4	8.88	6.0	30W p (40s), double n
451	LE SnO_2	826	14.5	71.5	8.58	4.8	10s 25W/28s 50W 2 step p, 0.45 um double n
452	LE SnO_2	824	14.6	73.0	8.77	4.9	10s 50W/35s 50W 2 step p, 0.45 um double n
456	LW SiO_2-SnO_2	834	15.4	68.2	8.73	6.2	
	LE SnO_2	828	15.2	68.0	8.55	5.5	

Note: "double n" denotes a (n a-Si:H)/(n uc-Si:H) bilayer.

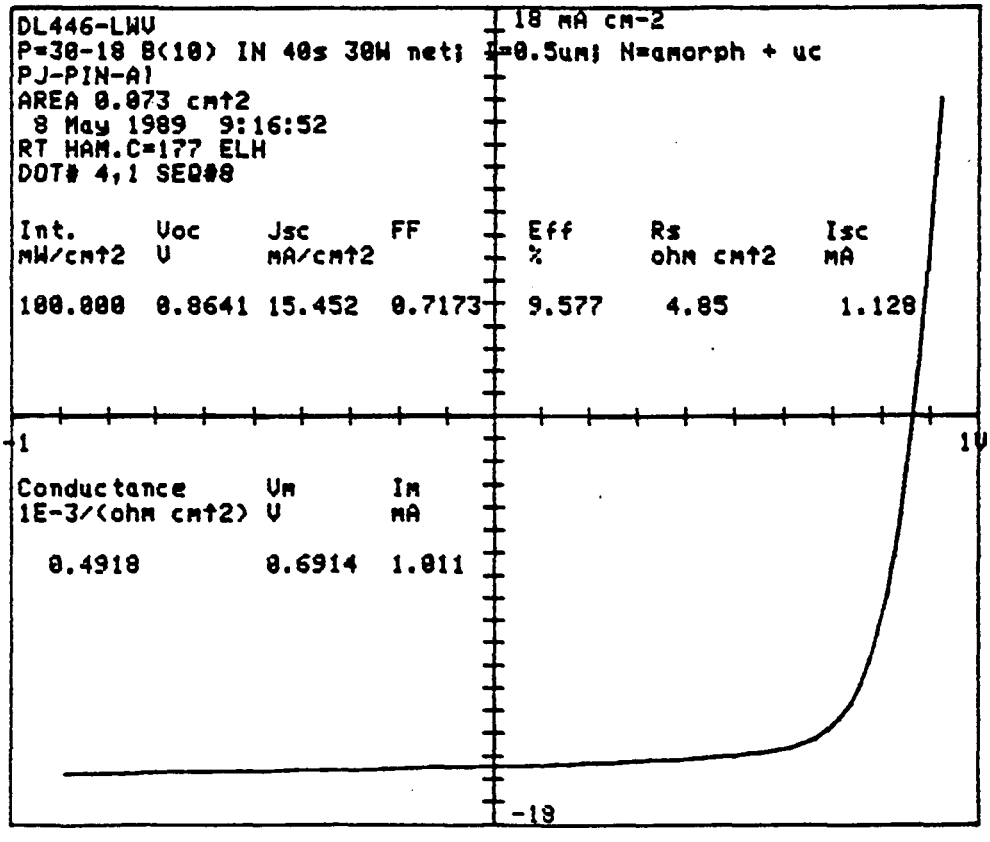

Fig. 1 J-V curve of a single junction cell on SnO_2 with modified p-layer. Cell efficiency 9.6%, Al metallization.

2.3 Single Junction Cells

Although the principal goal of this subcontract is to improve same bandgap, tandem junction cells and submodules, it is nevertheless a major component of the research to continue single junction cell work as a vehicle for the evaluation of various TCO options, the investigation of surface modification of the TCO's, p-layer development, and back reflector development.

Having discussed p-layer research in section 2.2, we focus in this section on an evaluation of device results obtained with various TCO coatings on glass, namely:

a. SnO_2

b. SnO_2/ZnO

c. SiO_2/SnO_2

Table III compiles the data for V_{OC} and J_{SC} for single-junction device runs in which simultaneous depositions were performed on glass/SnO_2 substrates and similar substrates in which the SnO_2 had been overcoated with 0.1-0.8 μm of sputtered Al-doped ZnO.

Table III. Comparison of V_{OC} and J_{SC} obtained with simultaneous deposition of p-i-n cells on SnO_2 and SnO_2-ZnO substrates.

Run #	V_{OC}(mV) SnO_2	V_{OC}(mV) SnO_2-ZnO	J_{SC}(mA/cm^2) SnO_2	J_{SC}(mA/cm^2) SnO_2-ZnO
405	842	866	15.0	15.5
424	796	820	14.2	13.8
425	828	854	14.5	14.1
428	823	842	15.1	14.9
431	830	892	13.7	12.1
433	754	831	14.7	13.6
442	814	827	15.8	14.1
Avs.	812	847	14.7	14.0

In all cases the V_{OC} for cells on ZnO exceeded the V_{OC} for comparison cells on SnO_2. The average V_{OC} obtained on ZnO was 847 mV compared to 812 mV on SnO_2. This unambiguous improvement in V_{OC} due to overcoating of the

SnO_2 with ZnO was in practice offset by a reduction in J_{SC} (14.0 compared to 14.7 mA/cm²) which we believe is principally due to optical absorption in the ZnO rather than a reduction in granularity. In any case, it would appear that the loss in J_{SC} could in the future be greatly reduced by making the ZnO overcoating much thinner, say 250Å. A valid comparison of fill factors obtained on the two types of substrate is more difficult to obtain because of the ambiguous effect of the oxygen plasma surface treatment on the fill factor of the SnO_2 cells. However, naive averaging of all the available data suggests that fill factors are roughly comparable for conventional cells on SnO_2 and cells on oxygen-plasma treated ZnO. We therefore conclude that overcoating of the SnO_2 with a very thin layer of ZnO should result in higher efficiencies. This would appear to be the case for run 428, (see Table II) in which the ZnO thickness was about 1000 Å, and the average dot efficiency was 8.7% compared to 8.2% on SnO_2. The J-V curve of the best small area cell on SnO_2/ZnO is shown in Fig. 2. Its efficiency is 9.0%.

Regarding the use of SiO_2/SnO_2, the limited number of comparisons available all indicate that cells on SiO_2/SnO_2 slightly outperform cells on the standard SnO_2 substrate, despite the fact that optimal SiO_2/SnO_2 is not yet available. This result is illustrated in Table II by the entries for run 456. We are therefore optimistic regarding future increases in efficiency through the use of SiO_2/SnO_2 and SiO_2/SnO_2/ZnO.

2.4 Tandem Cells

The new types of p-layer described in section 2.2 above have not yet been incorporated into tandem cells. Consequently, the best results obtained during the current reporting period for same bandgap tandem cells were comparable to those already achieved at the end of Phase II. Thus, in run 426, for example, average cell parameters were 1.65V, 7.54 mA/cm², FF 69.5%, Eff. 8.67% for small area cells. This current density was achieved using SnO_2-coated pyrex glass having a graded-index antireflection layer on the outer surface [3,4]. The boron content of the second stack p-layer was 25% larger than that used in the first stack p-layer, the latter being identical to the standard p-layer described in section 2.2. No interstack recombination layer was used in this cell. Experiments concerning such layers are described in section 3.3.

The external quantum efficiency of the top and bottom stacks of a typical tandem cell are shown in Fig. 3. In this example a ZnO/Cu back reflector is used.

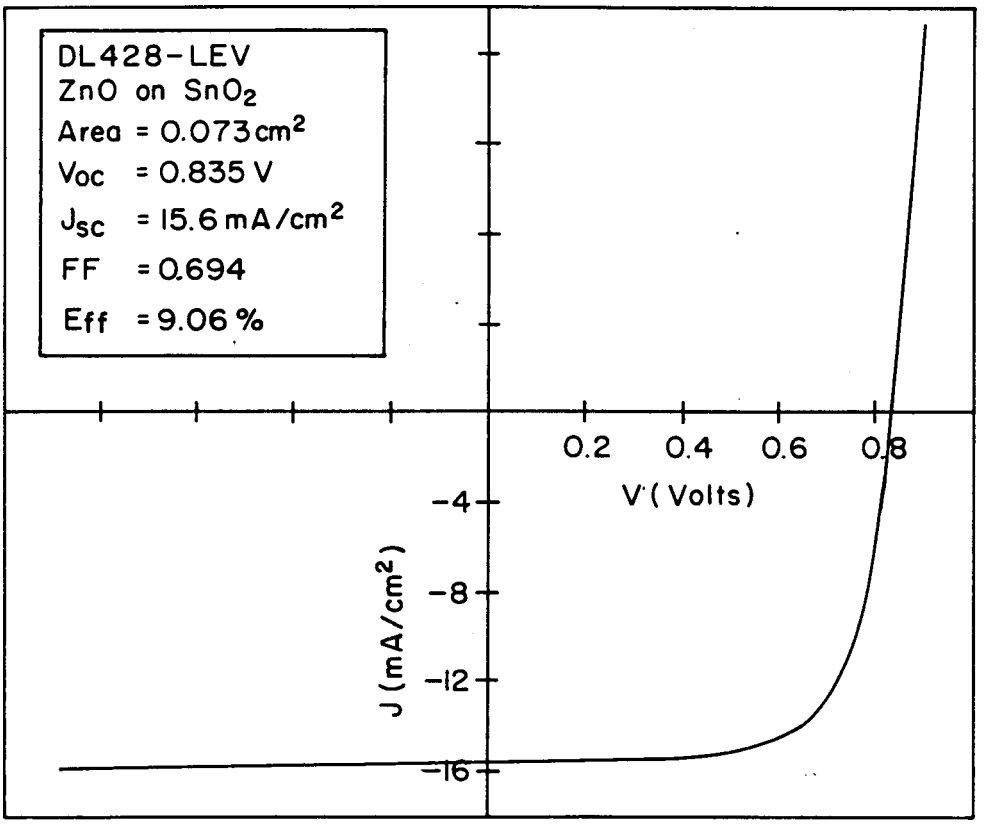

Fig. 2 J-V curve of a single junction cell prepared on SnO_2 overcoated with ZnO. Cell efficiency 9.1%, Al metallization.

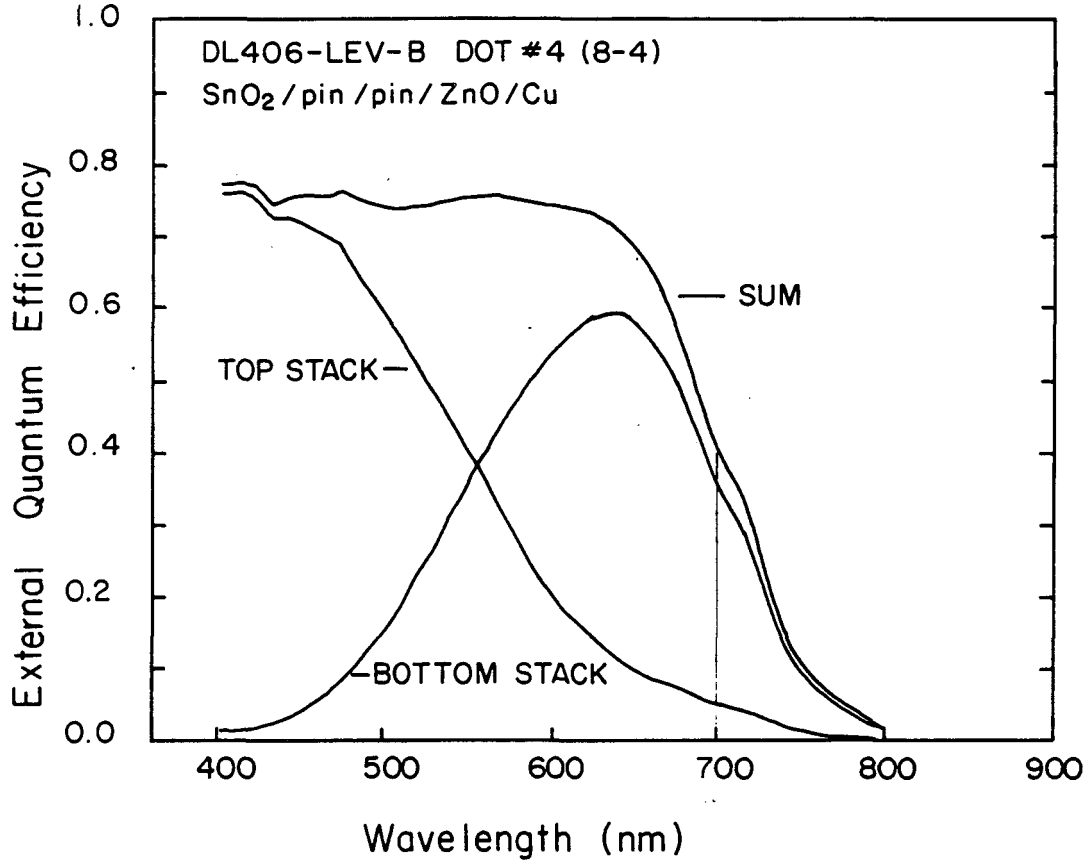

Fig. 3 External quantum efficiency of the top and bottom stacks of a tandem cell with a ZnO/Cu back reflector.

2.5 Techniques to Allow Changes in Back Contact Materials and Delayed Metallization

We have developed techniques to change the back contact/back reflector on completely assembled solar cells (recycling), as well as to allow successful delayed fabrication of a back contact/back reflector on solar cells after long times have elapsed since semiconductor deposition (during which time oxides and other materials build on the silicon surface).

Recycling techniques are useful in order to compare the performance of different back contacts. Techniques that allow successful delayed application of back contacts are useful, in a practical sense, since, for one reason or another, silicon that was never metallized often becomes an attractive metallization candidate.

With the recycling technique applied to an aluminized panel, the aluminum back contact is first removed with aluminum etchant. The silicon is then submerged in a solution of 1% hydrofluoric acid and water for 30 seconds, and the new back contact can then be applied. With this technique, solar cells measuring 71% fill factor were recycled, aluminum metallization to aluminum metallization, and the fill factors of the recycled cells measured 67%. We are improving on this technique, and hope to arrive at a method that would cause no degradation in fill factor.

For delayed metallization, certain commercially available cleansers can clean the silicon adequately before metallization (one such cleanser consists of sodium phosphate and sodium chromate). Another effective technique is to dip the silicon in a 1% solution of hydrofluoric acid and water for times in the range 10 seconds to 1 minute. The exact time is the time necessary to convert the silicon surface from hydrophilic to hydrophobic, and this time depends on the age of the silicon and the environment in which it was stored. Using these techniques, silicon that had been left out in the laboratory for one-half year was treated, then aluminized. Resulting J-V measurements showed fill factors (greater than 70%) equal to and exceeding fill factors of cells in adjacent areas of the silicon that had been metallized in a timely fashion. If no treatment of the silicon is employed we have found that the fill factor immediately after metallization declines by about 0.09% per hour that elapses between silicon deposition and metallization. (This factor applies for times up to 120 hours).

2.6 Cell Photostability

We report in this section results on three aspects of light induced degradation: subsection 2.61 deals with a spectroscopic technique (DLTS) for examining the gap state density as a function of light soaking, subsection 2.62 investigates the dependence of photodegradation on cell type, and subsection 2.63 describes a possible method for improving the stability of a-Si:H after it has been deposited.

2.61 Deep Level Transient Spectroscopy

Using DLTS, based on short-circuit current transients after repetitive excitation of p-i-n devices by light, we observe in all samples low and high temperature peaks at about 130K and 320K [1]. The latter peak corresponds to a trap depth of 0.8 eV; we assign this peak to dangling bonds, and its magnitude increases with light soaking. The former peak (trap depth 0.3 eV) decreases with light soaking.

We have previously reported that, as a cell is progressively light soaked, its i-layer collection length/thickness ratio (Lco/L) deduced from the 0.01 sun fill factor varies inversely with the i-layer dangling bond concentration deduced from current DLTS [3,5].

The reason for the decrease upon light soaking of the 0.3 eV peak is associated with tail states. We now argue that the increase in dangling bond density results in a smaller shift of the quasi fermi level into the tail states (upon excitation), which in turn results in decreased trapping, and hence accounts for the lower DLTS signal for the low temperature peak [6].

If the band tail density of states varies exponentially with energy with a characteristic slope ΔE, then the trapped charge in the band tail varies as $\exp(-E_F/\Delta E)$, and the observed ratio of the low temperature peaks for the annealed and light soaked conditions will be

$$I(0.3eV)_a/I(0.3eV)_s = \exp[(E_{Fs} - E_{Fa})/\Delta E]$$

$$E_{Fs} - E_{Fa} = kT \ln [D(0.8eV)_s/D(0.8eV)_a]$$

where D (0.8eV) is the density of states at E = 0.8eV. As reported at the 9th E.C. Photovoltaic Solar Energy Conference, the experimental data for several samples were found to be reasonably consistent with the above model [6].

2.62 Comparison of Photostability of Various Cell Types

Various cell types were selected for simultaneous light soaking in an attempt to isolate the factors that determine susceptibility (or resistance) to photodegradation. The variables considered in this study were a) junction type (single or tandem), b) thickness, c) top or bottom junction limitation, d) type of transparent conducting oxide as substrate, e) p-layer type, and f) i-layer deposition conditions. Twenty-nine as-deposited cells were selected, characterized, and mounted in a circle on a rotating turntable under a metal halide lamp. Slip-rings enable the signal from a monitoring photo-detector to be led from the turntable to an integrating totalizer for the determination of mean intensity. The cells were individually placed under resistive load at their maximum power point. Current-voltage curves under standard illumination were measured periodically. The light soaking was continued for a total of 571

hours. Pertinent data from this study are shown in Table IV.

Table IV. Efficiency loss of various cell types after 571 hours light soaking.

Junction type	I-layer thickness (nm)	Features	Efficiency initial (%)	Efficiency final (%)	change (%)
T	76/380	B.L. TiO_x	6.81	5.88	-13.7
T	57/285	TiO_x	7.00	5.64	-19.4
S	400	SnO_2-ZnO	8.21	6.37	-22.4
S	500	205°C	7.71	5.85	-24.1
T	70/700	T.L	8.15	6.07	-25.5
T	67/380	TiO_x	9.18	6.79	-26.0
T	83/700		7.71	5.41	-29.8
S	400		7.69	5.37	-30.2
S	500	SnO_2-ZnO	7.59	5.27	-30.6
S	500	standard cell	8.03	5.12	-36.2
S	350	high gas flow	7.95	4.33	-45.5

Note: Light soaking was conducted at 50°C, 0.94 suns, max. power point load.

B.L. denotes bottom-limited tandem

T.L. denotes top-limited tandem

TiO_x denotes TiO_x interstack layer

SnO_2-ZnO denotes ZnO-overcoated SnO_2 glass substrate

205°C refers to deposition temperature; standard is 180°C

The following observations were made:

a. For cells prepared under standard conditions on SnO_2, tandem cells are more stable than single junction cells and are capable of higher stabilized efficiencies. Stability generally improves with decreasing i or i_2-layer thickness. This agrees with the finding of an earlier study [3,4,7].

b. For tandem cells of equal bottom stack (i_2) thickness, top-stack or bottom-stack limitation appears to improve stability.

c. For single-junction cells of equal thickness, overcoating of the SnO_2 substrate with ZnO noticeably improves stability. (For 400 nm cells, the efficiency loss is 22.4% for SnO_2-ZnO versus 30.2% for bare SnO_2). It is of interest that the ZnO appeared to suppress the current loss on light soaking in preference to the fill factor loss.

d. Unusual i-layer conditions can strongly affect stability; good stability was observed for a 0.5 μm cell prepared at a higher than usual temperature (205°C), while surprisingly poor stability was observed in a thin (0.35 μm) cell prepared with an i-layer gas flow 1.75 x the normal flow rate.

e. No significant correlations could be made with p-layer type in single-junction cells, or presence/absence of a TiO_x interstack layer in tandem cells.

f. Larger than normal V_{OC} losses were observed in tandem cells having a 25% thinner p_2-layer. It is conceivable that this might be caused by n_1/p_2 interdiffusion.

In conclusion, the most remarkable finding of this study must be the observation of single-junction cells on SnO_2-ZnO having a stabilized efficiency (6.37%) second only to that of the best tandem junction cells (6.79%) on SnO_2.

2.63 Effect of Flash Irradiation/Anneal Treatment

We have conducted experiments in order to evaluate a proposed method for increasing the photostability of solar cells. In the past, we have observed (but never published) data that indicates a "hardening" effect, wherein light-soaked cells, after having been annealed in order to remove light-induced effects, exhibit increased resistance to subsequent light soaking.

Following the publication by Nevin et al., [8], in which presented data are interpreted as showing increased solar cell photostability following intense light pulse treatment and annealing at 160°C, we decided to re-examine the hardening question using both a high-intensity pulsed xenon source and an ELH source focused to 50 suns irradiation.

Such experiments conducted so far make use of a xenon lamp having a strobe frequency of 120 pulses/second, with a pulse duration of 6μs, and a peak irradiation of approximately 2800 suns. We further decided to perform the light flash treatment at the annealing temperature, in order that the easily annealed defects may be recycled many times (i.e., created, destroyed, created, destroyed...), increasing the probability of formation of a stable structure. (We hypothesize that there may be more than one distinct channel for atomic rearrangement that leads to the annealing of a defect, and that a stable configuration may be reached with some small probability, say, for 1 in 10^4 annealing events).

We found it necessary to maintain the cell at above 150°C, in order that the annealing rate relatively closely match the rate of photoinduced degradation. This determination was made by the use of J-V measurements at the flash/anneal temperatures. In these experiments, solar cells metallized with 500 Å titanium backed with 4,000 Å aluminum were used, in order to prevent interlayer diffusion between the amorphous silicon and the back

contact. High-intensity light flashing at the annealing temperature was maintained in the range 20 to 200 seconds.

The procedure was to flash/anneal the cells, as explained above, then light soak them under load, with irradiation of 0.8 suns, and temperature of 40°C. Cells that were exposed only to the annealing temperatures and as-deposited cells were also light soaked, serving as controls. In some tests, additional annealing for 30 minutes at the elevated temperatures was allowed past the period in which flashing occurred, and before light soaking. J-V measurements before and after light soaking were used as a means to evaluate photostability.

Cells given flashing treatment for 100 s and greater, and in addition, given the extra 30 minute annealing at 170°C, showed slightly improved photostability. These results are summarized in Table V, below, where data for both test and control samples are given, and the drop in efficiency listed is the drop from the as-deposited efficiency to the final efficiency after light soaking. The light soaking time for the cells was 76 hours, under the above-described conditions. Also in Table V, the annealing time given is made up of two parts. The first part is the real-time duration over which flashing occurred, which is four times the actual flash duration. This relationship occurs because the above-mentioned duty cycle for flashing was maintained for four seconds, interrupted by a 16 second wait (in order that the strobe power supply not overheat). The second part of the annealing time of Table V is due to the 30 minute additional annealing period.

Table V. Effect of flash irradiation/anneal on photostability

Run #	Irradiation time[a] (s)	Total anneal time (s)	Drop in efficiency[b] (%)
2	0	800 + 1800	36.1
	200	800 + 1800	34.5
4	0	400 + 1800	35.2
	100	400 + 1800	31.7

a. Time during which flashing occurred; actual irradiation time is 6μs x 120 s^{-1} per second of flashing.

b. Light soaking was performed at 1 sun, 50°C, open-circuit conditions, for 76 hours.

We thus conclude that cells subjected to both a minimum flashing treatment and sufficient subsequent annealing can show some improvement in photostability. Further experimentation is however necessary in order to firmly establish that such post-fabrication treatment significantly improves the photostability of solar cells.

3.0 NON-SEMICONDUCTOR MATERIALS

With the objective of maximizing the performance of each independent component of the solar cell, we discuss here our efforts regarding the deposition and characterization of non-semiconductor materials, specifically the transparent conductors. Tin oxide films were characterized in terms of their electrical and optical properties. Aluminum-doped zinc oxide films were prepared under different conditions and were characterized exhaustively. The performance of solar cells using this material as a substrate were reported in section 2.3. Further discussion of the use of ZnO in device applications is given in subsections 3.24 - 3.27 below. These subsections describe the necessity of surface treatment of the ZnO before its use as a substrate for a-Si:H deposition, the thermal stability of cells having ZnO as a back contact, the production of granular ZnO, and the use of ZnO as a back reflector.

3.1 Tin Oxide

At Chronar, two tin oxide coatings are in use. Both processes use tin tetrachloride as the tin source and both involve the deposition of two layers. In the first process both layers are tin oxide. The first layer has no dopant. However, additives are included in the reactant gas mixture to facilitate a more uniform nucleation of the tin oxide. The second layer uses a fluorinated hydrocarbon in the gas mixture to yield a fluorine-doped tin oxide layer.

In the second process at Chronar, first a thin layer of silicon dioxide [9] is deposited as a barrier layer, then a doped tin-oxide layer is deposited in a similar (but not identical) fashion to the second layer of the first process.

The advantages of each technique are summarized below. First, the advantages of direct deposition of tin oxide on soda lime glass are: 1) there is a somewhat larger tin oxide growth-rate, and 2) hazy coatings (desirable for solar cells) are more easily obtained. The advantages of adding a barrier layer are: 1) The sodium content of the tin oxide film is much lower. 2) Much less dopant is required for a given tin oxide conductivity [9]. In fact, only in the case of a barrier layer were we able to obtain conductivities on the order of 3000 $(\text{ohm-cm})^{-1}$ [9]. 3) Better coverage is obtained (without the barrier layer, thin layers of tin oxide on soda lime glass tend to be full of pinholes). 4) Less rigorous cleaning of the substrate is required for reproducible results.

The properties of various tin oxide samples, both Chronar-produced and from outside, were compared. Table VI summarizes their electrical and optical characteristics. The Chronar-produced samples are designated PJ (glass/SnO_2) and EMF (glass/SiO_2/SnO_2).

Table VI. Characterization of various tin oxide coated glass.

Sample source	Sheet resistance (ohms/sq.)	(A)	Total Thickness (ohm cm)	Diffuse Resistivity (%)		Plasma wavelength (nm)	Carrier concentration (cm^{-3})	Mobility cm^2/Vs
EMF	15.8	4400	6.95×10^{-4}	80.50	1.05	3400	1.08×10^{20}	83.26
EMF-B	19.8	3600	7.12×10^{-4}	79.12	0.62	4100	7.44×10^{19}	117.9
EMF-A	12.8	5300	6.78×10^{-4}	78.35	1.35	3000	1.39×10^{20}	66.32
PJ	12.5	7000	8.75×10^{-4}	77.21	7.77	2500	2.00×10^{20}	35.71
PILK.	16	4200	6.72×10^{-4}	76.20	< 0.1	3400	1.08×10^{20}	86.11
LOF	13.9	4300	5.97×10^{-4}	76.17	< 0.1	3400	1.08×10^{20}	96.93
AFG	11.0	8500	9.35×10^{-4}	71.74	0.75	2000	3.13×10^{20}	21.56
EMF 12/1/217D	31	3400	10.5×10^{-4}	79	2.8	NA	NA	NA
EMF 12/1/217C	17	4500	7.65×10^{-4}	78	2.8	NA	NA	NA
EMF 12/1/78C	14	5200	7.28×10^{-4}	79	1.6	3900	8.21×10^{19}	104
EMF 12/1/78D	23	3450	7.93×10^{-4}	81	0.97	3800	8.65×10^{19}	91
LOF-II	13	4300	5.6×10^{-4}	77	1.2	2900	1.49×10^{20}	75
NIPPON	8.1	NA	NA	79	5.3	2700	1.71×10^{20}	NA

The sheet resistance of the films was measured with a four point probe. The thickness of the sample was measured using a profilometer on a step etched on the samples. Using an electrochemical process, the film was made the cathode, and a stainless steel rod was used as the anode with diluted hydrochloric acid used as the electrolyte. The film is reduced to elemental tin, which can be easily removed. The electrolytic process is self-limiting, as the etching of the film stops the flow of current.

The total and diffuse transmission of the films were measured with a 60 cm integrating sphere and a white light source from which the infrared radiation had been removed. The plasma frequency was obtained from the transmission spectrum, and the carrier concentration was calculated from Drude's free electron theory as:

$$n = \omega^2 m^* \epsilon_0 \epsilon_1 / e^2$$

The mobility was calculated from the carrier concentration and resistivity as:

$$\mu = 1/e \rho n$$

Initial photovoltaic data for cells deposited on the various types of tin oxide are consistent with the data shown in Table VI. We have, in fact, obtained superior cell data for EMF substrates (glass/SiO_2/SnO_2) compared to PJ substrates (glass/SnO_2), see Table II, run #456.

3.2 Zinc oxide

Zinc oxide is a transparent, wide bandgap material which can be made conductive by non-stoichiometry and/or by doping with group III metals [10-12]. The high transmission and low sheet resistance of thin films of zinc oxide make it a useful transparent conductor for solar cell applications. As a front contact, it is distinguished from tin oxide by its stability in hydrogen plasmas. Particularly as a back contact, zinc oxide offers advantages over ITO with comparable sheet resistance and transmission, mainly for the following reason. Low fill factors for cell structures with ITO may be caused by indium diffusion into the a-Si:H n-layer. Even though one of the methods for producing high-conductivity zinc oxide involves doping with aluminum, the group III metal concentration is much less than in ITO.

Zinc oxide films can be produced by a variety of techniques. For this study we have applied rf magnetron sputtering using argon as the sputtering gas. The zinc oxide target is doped with aluminum oxide; the sputtered film thickness could be varied by changing either the speed of substrate movement, or the power input to the plasma.

The films prepared were characterized for their resistivity using a four point probe and a profilometer to measure the thickness. The optical transmission was measured with a spectrophotometer. The composition was analyzed by Auger electron spectroscopy. Our films exhibit high optical transmission and very low absorption over the visible spectral range (see Fig. 4). The film conductivity is on the order of 1 x 10^3 S/cm; it increases with the film thickness (see Table VII).

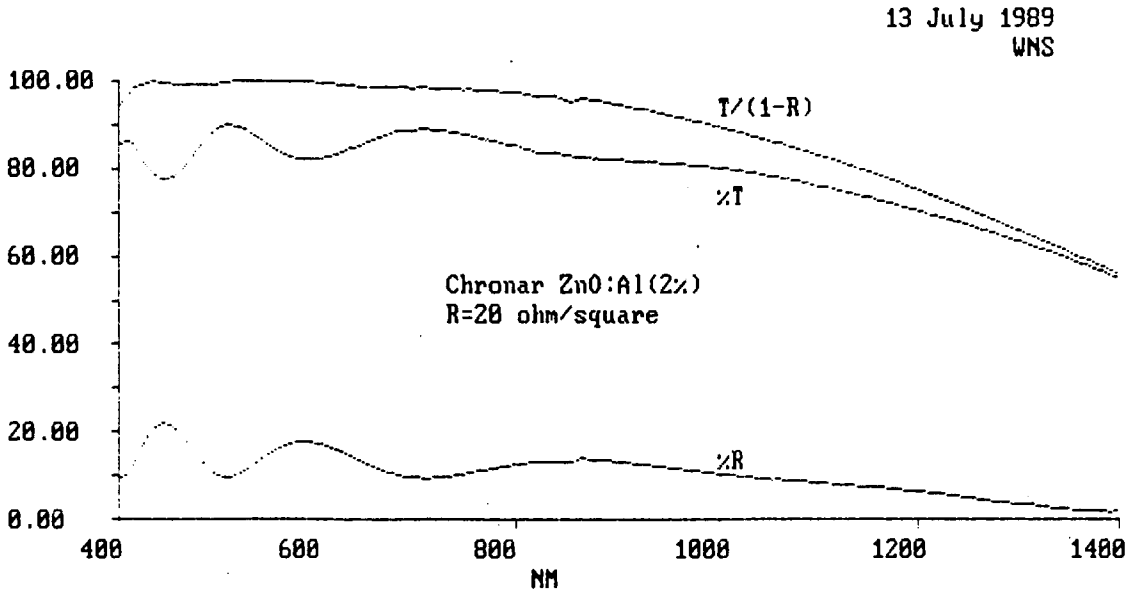

Fig. 4 Transmission and reflection spectra for sputtered ZnO:Al (measured at the Institute of Energy Conversion, University of Delaware).

Table VII: Effect of deposition conditions on film characteristics of zinc oxide (1% Al_2O_3).

Sample	Power (kW)	Scan speed (cm/min)	Thickness (nm)	Sheet resistance (ohms/sq.)	Conductivity S/cm
11/29-2	1	4	280	30.1	1.19×10^3
11/29-3	1	2	500	12.5	1.6×10^3
12/4-1	0.5	1	300	30	1.11×10^3
12/4-2	0.5	2	150	70	0.95×10^3
12/4-3	0.5	4	100	270	0.37×10^3

The film composition for both doping concentrations is nonstochiometric, i.e. metal-rich, which may contribute to the high conductivity. The Auger results also show lower zinc and dopant concentrations towards the film surface (see Table VIII).

Table VIII: Auger analysis of Zinc Oxide

Depth nm)	Zn %	O %	Al %	Total impurities (C, Cl)%	Value of x in ZnO_x
Sample 11/29-3	Target: ZnO 1 wt% Al_2O_3				
10	63.6	26.3	0.2	9.9	0.41
110	67.8	28.7	0.8	2.7	0.42
210	69.4	29.7	0.9	0	0.43
Sample 10/27-1	Target: ZnO 2 wt% Al_2O_3				
Depth (nm)	Zn %	O %	Al %	Total impurities %	Value of x in ZnO_x
10	68.7	26.5	1.1	3.7	0.385
110	70.9	27.1	2.0	0	0.382
210	70.9	27.1	2.0	0	0.382

3.21 Optical and electrical characteristics as a function of doping

The optical and electrical characteristics of doped zinc oxide films can be explained using Drude's free electron theory. The aluminum atoms increase the free electron concentration of the films by donating electrons to the conduction band. This increase in the free electron concentration with the concentration of the dopant manifests itself in the optical transmission spectrum as an increase in the plasma frequency and an increased absorption in the near-IR region. This is illustrated in Fig. 5, which shows the transmission versus wavelength for ZnO films prepared with 1 and 2 wt.% Al_2O_3 as dopant source in the sputtering target. The properties of these films are compared in Table IX.

Table IX: Comparison of properties of ZnO(1% Al_2O_3) and ZnO(2% Al_2O_3)

Sample #	Target Composition Al_2O_3%	Resistivity ($ohm^{-1}cm^{-1}$)	Plasma wavelength (nm)	Carrier concentration (cm^{-3})	Carrier mobility (cm^2/Vs)
11/29-3	1	6.25×10^{-4}	3500	1.2×10^{20}	83
4/6-2	2	4.8×10^{-4}	2000	3.0×10^{20}	43

The increase in the dopant concentration affects also the carrier mobility due to increased impurity scattering. Conversely, reducing the dopant concentration from 2% to 1% does not significantly affect the resistivity, but gives much better near-IR transmission. This could also be beneficial, if the migration of the dopant into the a-Si:H is the reason for the sporadic fill factor reduction problem.

3.22 Hall effect measurement

Hall effect measurements were carried out on aluminum-doped zinc oxide samples with a steady magnetic induction of 2500 gauss. The Hall coefficient R is defined as:

$$R = 10^8 \, V \, t \, / I \, B \quad cm^3/C$$

where V is the transverse Hall voltage (V)
t is the film thickness (cm)
I is the current (A)
B is the magnetic induction (gauss)

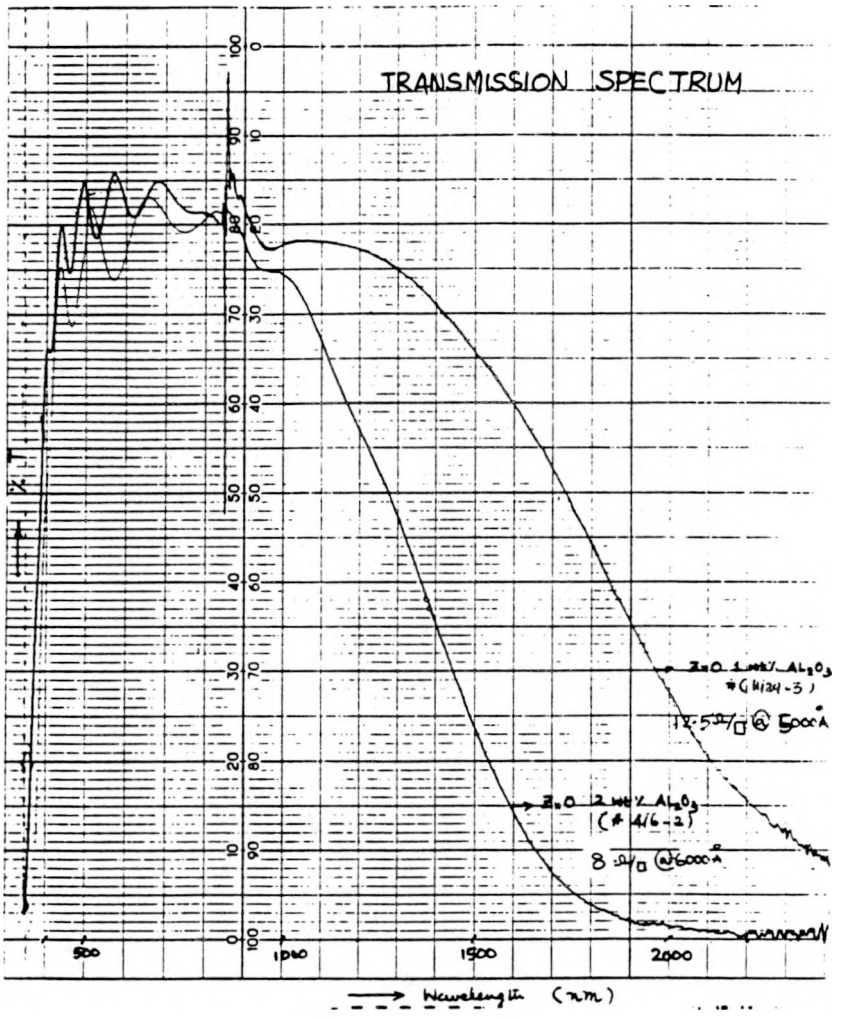

Fig. 5 Transmission spectrum for sputtered ZnO from differently doped ZnO:Al_2O_3 targets (1 and 2 wt.%).

The carrier concentration can then be found from

$$R = -1/nq \quad \text{(for electrons)}$$

This yielded a carrier concentration of $5.2 \times 10^{20}/cm^3$. The calculation of the carrier concentration from the transmission spectrum yielded $3.0 \times 10^{20}/cm^3$, in reasonable agreement. The data are summarized below:

Hall Measurement

Sample	4-5/2
Sheet resistance	5.4 ohms/sq.
Thickness	750 nm
Current	5mA
Magnetic induction	2500 gauss
Hall coefficient	$-0.012\ cm^3/C$
Carrier concentration	$5.2 \times 10^{20}/cm^3$
Mobility	$29.7\ cm^2/Vs$

Spectrophotometric Measurement

Plasma frequency	2000 nm
Carrier concentration	$3 \times 10^{20}/cm^3$
Mobility	$51.4\ cm^2/Vs$

3.23 X-ray Diffraction Analysis

X-ray diffraction analysis was performed on 1% and 2% wt. Al_2O_3 doped ZnO samples. Copper Kα radiation with a wavelength of 1.54 Å was employed. The samples showed relatively sharp peaks at $2\theta = 34.4°$, see Fig. 6. This is consistent with the crystal structure of ZnO (zincite) which is hexagonal or wurtzite (a = 3.249 Å, c = 5.205 Å). The peak corresponds to the 002 (hkl) reflecting plane, with an interplanar spacing of c/2 or 2.602 A. The absence of other peaks indicates a strong (002) preferred orientation. From the FWHM of 0.3° we may estimate the crystallite diameter d (in a direction normal to the reflecting planes) using the formula

$$d_{hkl} = \frac{0.9\ \lambda}{\Delta(2\theta)\cos\theta}$$

This gives a crystallite size of 280 Å.

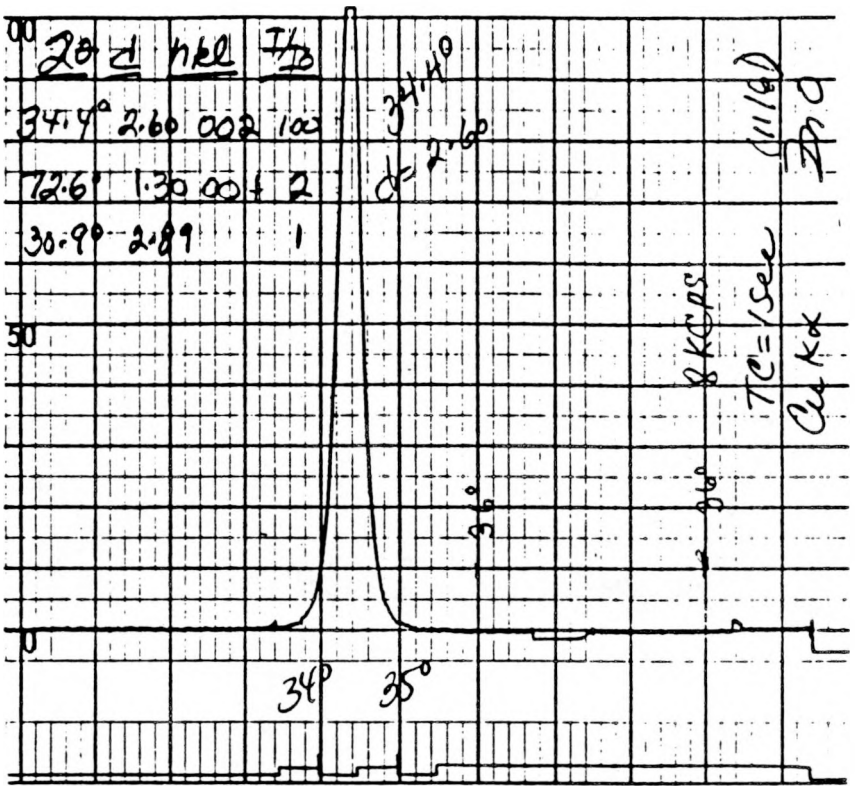

Fig. 6 Powder X-ray diffractogram of sputtered ZnO.

3.24 Effect of TCO Surface Treatment on Cell Performance

In depositing the amorphous silicon for a p-i-n cell, it is customary to clean the surface of the SnO_2 in situ using an Ar discharge before initiating deposition of the p-layer. If this step is omitted, cell performance is inferior and variable. We believe that one effect of the Ar discharge is to very slightly reduce the surface of the SnO_2, thereby forming a small quantity of free tin, and that this results in a reliable, low resistance contact to the p-layer. However, we have found that this procedure does not work for SnO_2 overcoated with ZnO [3,4]; the solar cells are found to have a low fill factor (see data for run 405 in Table II). It was deduced that the low fill factor results from an unacceptably large ZnO/p-layer contact resistance.

We therefore decided to try to reduce this contact resistance by experimenting with alternative surface modification procedures applied to the ZnO. It was discovered that treatment of the ZnO in an oxygen-containing plasma prior to p-layer deposition allowed the formation of high quality p-i-n cells. In particular, in run 424, both SnO_2-ZnO and SnO_2 substrates were subjected to a 15 minute, 40 watt Ar discharge followed by a 5 minute, 25 watt discharge of 30% O_2 in Ar (flow rate 30 sccm, pressure 200 mTorr), resulting in average fill factors of 73.1% and 66.9%, respectively, and efficiencies of 8.25% and 7.54% on the SnO_2-ZnO and SnO_2 substrates (see Table II). In run 428, an average efficiency of 8.70% was attained on a SnO_2-ZnO substrate using a 3 minute discharge of 30% O_2 in Ar. The underlying reason for the reduction of the ZnO/p-layer contact resistance is not clear, for a lowering of the oxygen vacancy concentration near the ZnO surface might be expected to reduce the surface conductivity of the ZnO.

Table X. Series resistance observed in p-i-n cells as a function of substrate type and plasma treatment.

	R_s (= dV/dJ @ V_{oc}) ohm cm^2	
discharge	SnO_2	SnO_2-ZnO
Ar	4.8 - 7.0	21.1
30% O_2 in Ar	4.4 - 6.6	4.4 - 4.9
H_2	5.2	5.8

Table X consolidates our observations regarding the dependence of R_s (defined as dV/dJ @ V_{oc}) in single junction cells on a), substrate type (SnO_2 or SnO_2-ZnO), and on b), the type of discharge used for surface treatment prior to p-layer deposition. While there are three contributions to R_s, namely, contact resistance at the TCO/p-layer interface, diode resistance, and contact resistance at the n-layer/Al interface, the

latter two contributions are expected to be constant. Consequently, variations in R_s are attributed to variations in the TCO/p-layer contact. These variations in R_s directly affect fill factor, as can be seen in the data of Table II. The oxygen plasma treatment of ZnO, which enables fabrication of cells with high fill factors, is clearly an important discovery.

Additional work in this area will be necessary to optimize this type of surface modification and to understand the underlying physics.

3.25 Thermal Stability of Cells Prepared with ZnO

The thermal stability of cells provided with ZnO as back contact material was evaluated, and the results are shown in Table XI below:

Table XI. Dependence of photovoltaic data on heat treatments for cell with ZnO back contact.

	V_{oc} (V)	J_{sc} (mA/cm²)	FF	Eff (%)	R_s (ohm-cm^2)
before anneal	0.786	14.08	0.724	8.02	4.24
+ 24h @ 85°C	0.787	14.11	0.723	8.02	4.63
+ 24h @ 85°C	0.790	14.17	0.723	8.08	4.69
+ 48h @ 102°C	0.784	14.15	0.718	7.97	4.49
+ 72h @ 140°C	0.794	13.68	0.707	7.61	5.68

These preliminary results indicate that cells with ZnO back contacts have similar thermal stability as those with regular Al back contacts.

3.26 Granular ZnO

The ZnO films prepared by r.f. magnetron sputtering were quite specular, with only slight texture developing in thick films deposited at elevated temperatures. Several attempts were made to induce granularity in order to increase the light trapping in the solar cells. Successful methods are:

1. Deposition of ZnO on granular tin oxide,

2. Sputter-etching of the film after deposition,

3. Wet etching of the film in diluted acids.

The most successful of these methods was the wet etching technique. The sample was dipped in a dilute (< 5% HCl) acid solution. The etch rate is a function of the orientation of the crystallites and hence the etched sample scatters light. The amount of light scattering can be easily controlled by

varying the etch time. The roughness of the sample surfaces was characterized by scanning electron microscopy (Fig. 7); diffuse optical transmission was measured by using a 60 cm integrating sphere with a white light source from which the infrared radiation was removed (see Table XII). An etch time of 20 secs (sample # 07/17-2) in 3% HCl resulted in optimum diffuse transmission (around 7-10%).

Table XII: Optical and electrical characteristics of ZnO:Al films before and after wet etching.

Sample #	Etch time	Sheet resistance		Direct light photocurrent		Scattered light photocurrent	
		before	after	before	after	before	after
	(sec)	(ohms/sq)		(uA)		(uA)	
07/17-1	10	17 - 18	22 - 24	35 - 40	39-41	0.3 - 0.4	1.2 - 1.3
07/17-2	20	20 - 22	30 - 54	38 - 41	36 - 39	0.3 - 0.4	3.5 - 4.3
07/17-3	30	20 - 22	500 - 2000	39 - 41	39 - 40	0.3 - 0.4	7.0 - 8.0

3.27 ZnO-Based Back Reflectors

We investigated ZnO in back contact combinations, such as ZnO/Al, ZnO/Cu, ZnO/Ag, and ZnO/$BaSO_4$-paint. In all cases, and in comparison to straight Al, an increase of short-circuit current is observed, while the fill factor may be slightly lower, but not always. We suspect that the fill factor decrease is caused by a higher contact resistance between the n-layer and ZnO, possibly by Al dopant diffusion from the ZnO. Table XIII shows the photovoltaic data with three different back contact combinations, deposited onto the same cell structure (run DL446). A 3-pass method was employed for the ZnO.

Table XIII. Dependence of photovoltaic data on the back contact material

Back Contact	V_{oc} (V)	J_{sc} (mA/cm²)	FF	Eff (%)	R_s ohm-cm²
ZnO/Cu	.789	15.52	0.716	8.76	4.19
ZnO	.803	14.84	0.678	8.07	5.76
Al*	.782	13.83	0.701	7.59	5.29

*The Al was deposited considerably later than the ZnO.

The observed increase in the short-circuit current is typically due to improved red response. Thus the quantum efficiency at 700 nm increased from

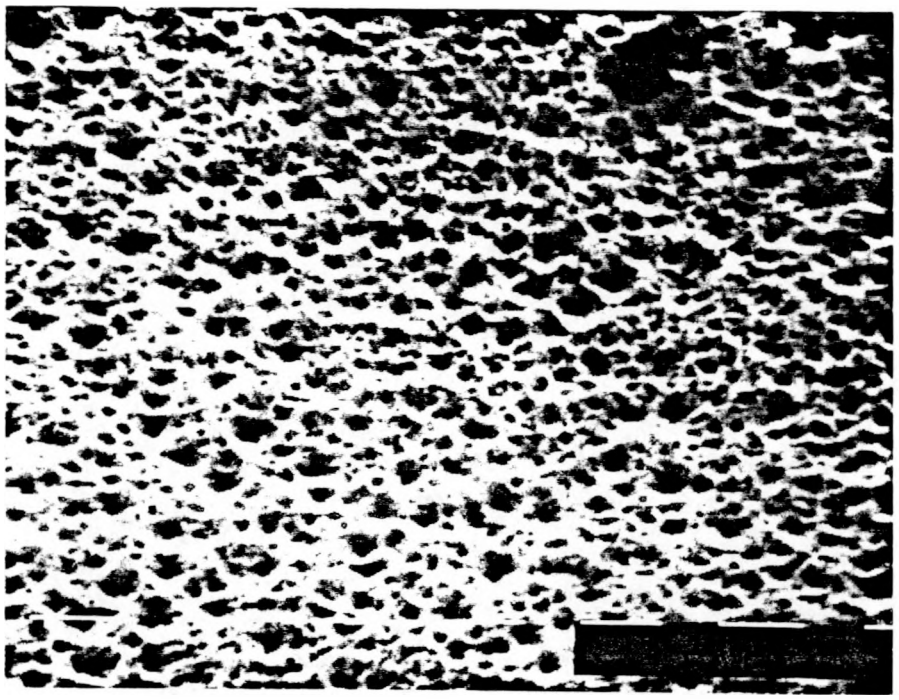

Fig. 7 Scanning electron micrograph of sputtered ZnO, chemically textured (magnification 10kX, 30°, sample 07/17-2).

0.28 to 0.42 for a small-area cell with Al and ZnO/Cu reflectors, respectively. As a further example, Fig. 8 shows QE (700nm) = 0.46 for a cell with ZnO/$BaSO_4$ back contact; this particular cell yielded an efficiency of 8.8%.

3.3 Interstack Layers in Tandem Cells

We have previously reported that the V_{oc} and FF of tandem (p-i-n/p-i-n) cells can be improved through the use of an interstack layer whose function is apparently to facilitate electron-hole recombination at the central n/p junction [3,4,7]. The interstack layer was prepared by thermal evaporation of titanium sesquioxide, thereby yielding a conductive sub-oxide TiO_x. In order to determine the influence of TiO_x deposition conditions on tandem cell performance, the LW, LE, and RE plates of run DL423 received 80A TiO_x layers under the following conditions (base pressure, evaporation rate) and with the following results:

LW	2.5×10^{-6} Torr	1.3 - 2.0 A/s	1.61V	6.79 mA/cm^2	FF 0.727	7.96%
LE	2.0×10^{-6} Torr	0.2 - 0.5 A/s	1.61V	6.90 mA/cm^2	FF 0.728	8.11%
RE	8.0×10^{-6} Torr	1 - 1.5 A/s	1.58V	6.73 mA/cm^2	FF 0.730	7.76%

We conclude that evaporation conditions for the TiO_x layer do not significantly affect cell performance.

4.0 SUBMODULE RESEARCH

In this reporting period, progress was made in the following areas of submodule research: 1) laser/etch isolation of the back contact, 2) distributed contact interconnection, 3) large-area shunt removal, and 4) fused interconnection by means of a laser. Techniques to allow both changes in back contact materials and delayed metallization were reported in section 2.5.

4.1 Laser/Etch Isolation of the Back Contact

We have developed a reliable technique that greatly increases the permissible range of laser operating parameters during isolation of the back contact. This technique has proven itself to be suitable for R&D activity, and with this technique, the laser isolation process becomes a minor factor in submodule processing difficulties.

In this technique, photoresist is applied to the back side of the panel just prior to lasering. After lasering, which patterns the a:Si/Al/photoresist layers, the plate is immersed in aluminum etchant. The resulting etching removes any shunt-producing aluminum flakes left behind after lasering. After etching, the photoresist can be removed. The final step is to subject each cell to current blasting, which ensures that no scribe-related shunts remain.

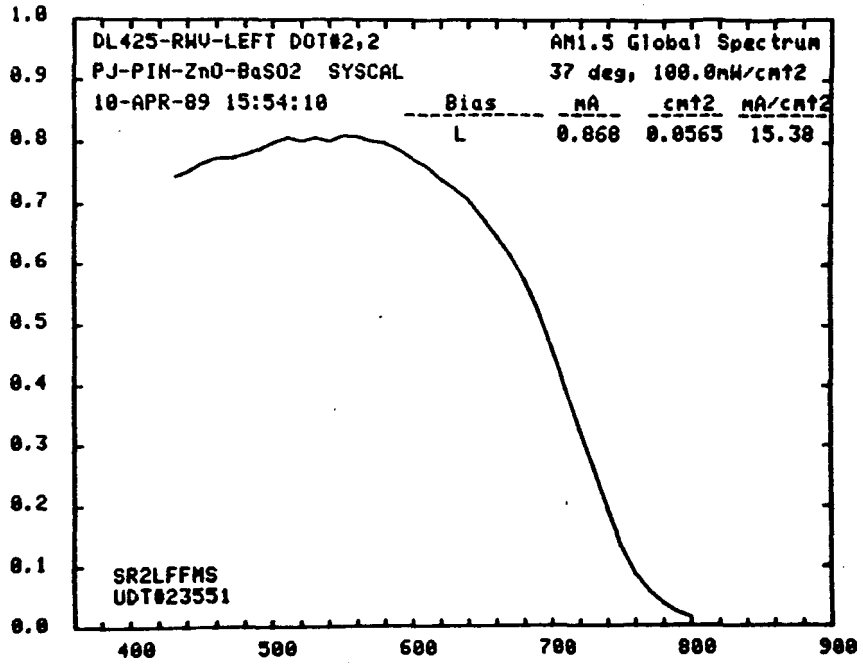

Fig. 8 Quantum efficiency with improved red response due to a $ZnO/BaSO_4$ back contact combination.

Processed in this way, panel DL444RWV yielded the following measured values: V_{OC} = 47.2 V, I_{SC} = 188 mA (6.71 mA/cm²), FF = 0.63, Eff = 6.65% (aperture area basis), and P max = 5.60 W. The I-V curve is shown in Fig. 9.

4.2 Distributed Contact Interconnection

The distributed contact interconnection scheme has been explained in previous publications and reports [3,4,7] with emphasis on the dot contact version of this scheme. The ultimate goals of this work are to obtain high area utilization and more flexibility in choice of submodule current/voltage combinations. Here, we report progress on the dash contact version of this scheme (see Fig. 10). The dash contact scheme can be thought of as equivalent to the dot contact scheme with the dots elongated in the form of dashes. The dash contact scheme has the advantage that the dashes can be made by existing lasering equipment.

The fabrication procedure developed for the dash-contact scheme is as follows:

1. Wash unscribed SnO_2/a-Si:H/Al_1 panel
2. Spray photoresist
3. Soft bake at 100°C for 1/2 hour
4. Define unit cells with 1.06μm laser
5. Etch panel in aluminum etchant
6. Current blast each cell
7. Respray with photoresist
8. Soft bake at 100°C for 1/2 hour
9. Scribe line-contact pattern with 0.53μm laser, exposing SnO_2
10. Expose photoresist in desired pattern
11. Hard bake at 100°C for 1/2 hour
12. Etch panel in aluminum etchant
13. Current blast each cell
14. Develop photoresist
15. Metallize with Al_2, in desired pattern

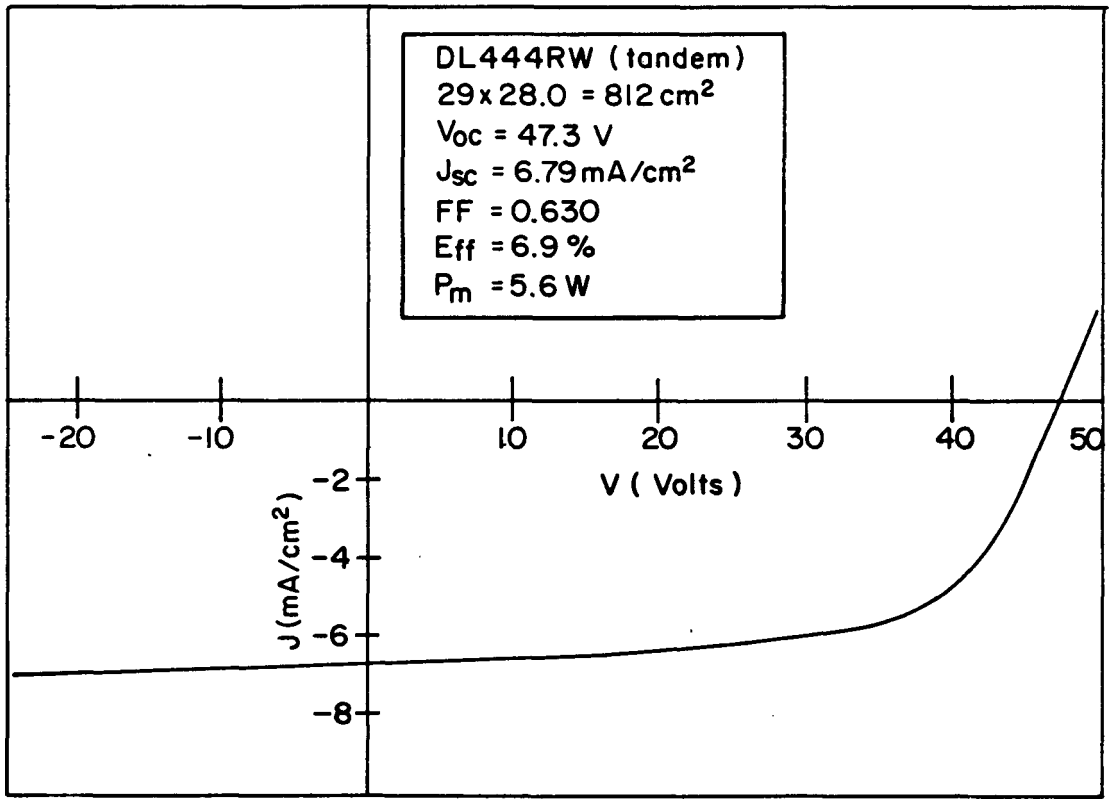

Fig. 9 J-V curve of a 5.6 watt, 1 ft.sq. tandem submodule employing the laser/etch isolation process.

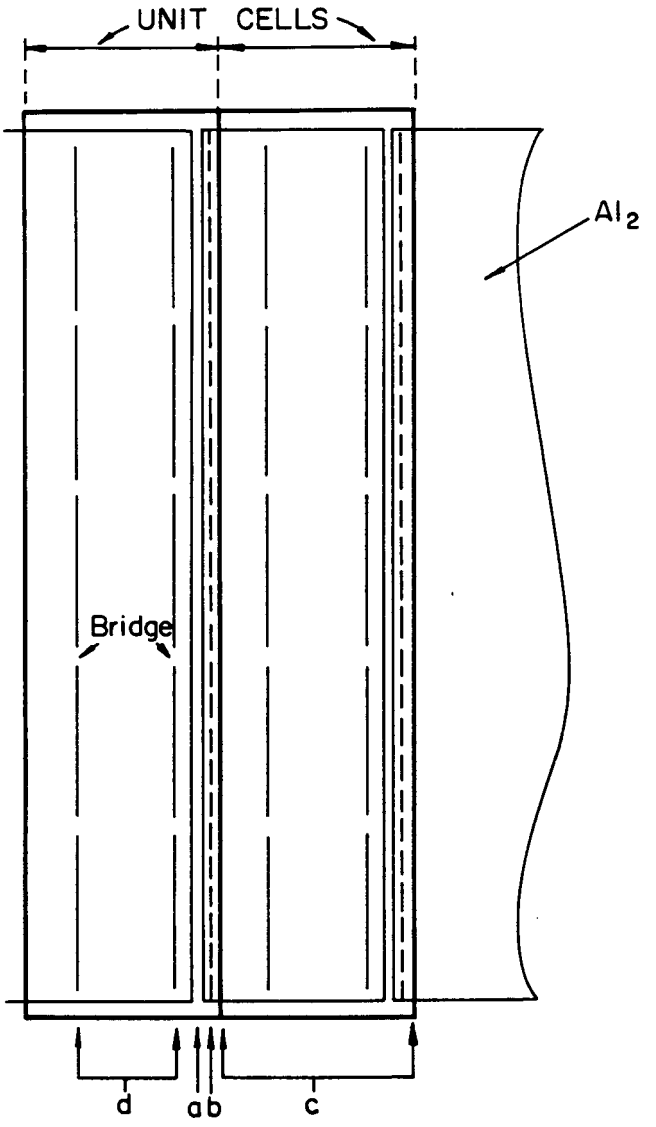

Fig. 10 Plan view of a dash-contact submodule showing the unit cells, and Al_2 layer as though transparent. a: Al_2 patterning, b: insulator scribe (to allow Al_2/Al_1 interconnect), c: unit cell scribe (through SnO_2/a-Si/Al_1), d: two rows of dash-contacts (Al_2-SnO_2 contact).

Panel DL321RWV was the first 1 x 1 ft.^{2} panel fabricated according to the dash-contact scheme. This panel contains a single junction cell, and the interconnection consists of 29 series-connected cells. The performance of the completed panel was poor, most likely due to shunting caused by Al_2 making contact through the tunnel left after acid etching and undercutting of Al_1. In order to avoid this shunting, three-scribe and modified single-scribe methods were proposed.

With the three-scribe technique, three 1.06μm laser scribes are made alongside each other in step 4, above. The 0.53μm laser scribe of step 9 is then made down the center of this triple-wide scribe. Panels DL430REV and DL430LEV were fabricated according to the three-scribe technique. These panels contain 2-junction cells, with 15 series-interconnected cells.

After current blasting of the completed DL430REV panel, measurement yielded V_{OC} = 19.3 V, J_{SC} = 6.35 mA/cm^2, fill factor = 45.7%. efficiency = 3.2%, and maximum power 2.82 W. The best cell of this panel measured 4.9% efficiency. After elimination of shunts, the best cell of DL430LEV dash-contact panel measured V_{OC} = 1.64V, J_{SC} = 6.68 mA/cm^2, fill factor = 51.7%, efficiency = 5.7%.

Performance of these panels is limited because of excessive series resistance and shunting. The series resistance is due primarily to the Al_2 contact (step coverage resistance of Al_2 was acceptable). The shunting is most likely due to unwanted removal of photoresist, exposing Al_1, which then shunts to Al_2. This unwanted removal probably occurs because of stray light exposure to the edge of the photoresist near the 0.53μm laser scribe, which in turn causes this edge to be removed during developing of the photoresist. Thus, a modified single-scribe technique was devised, in order to eliminate this shunting.

The fabrication procedure for this modified technique follows the above procedure in the sequence, 1, 2, 3, 4, 9, 5, 6, removal of photoresist and reapplication of photoresist, 8, 10 (with a step to expose the 0.53μm scribe lines from the front side of the panel), 11, 14, and 15. The front-side exposure of the 0.53μm scribes in step 10 will cause removal of photoresist from the SnO_2 during development of the photoresist, and because of the undercutting of Al_1 in step 5, no photoresist will be removed from the undercut tunnel, and thus, Al_1 will remain insulated from Al_2. We have not yet completed a panel with this modified technique.

4.3 Large-Area Shunt Removal

In the past, we have developed techniques that eliminate shunt-producing defects in panels with minimum damage to the panel. These techniques, however, have been labor intensive, primarily because the techniques require the shunting defect to be first made visible. We have thus made efforts to develop a less time-consuming process, - a technique that would allow rapid defect removal on large area panels (square foot and larger). Although results to date are not completely satisfactory, progress has been made, and further work is needed.

With the rapid method under investigation, the entire panel is submerged in an electrolyte, and each cell of the series-connected string is placed in reverse bias for a few seconds. Thus, each cell experiences the electrolyte for several minutes, a few seconds of which with a reverse bias.

The following electrolytes were studied: Type A aluminum etchant, aluminum chloride, ammonium chloride, boric acid, chromium chloride, nickel chloride, sodium chloride, and tin chloride. All solutions were 5% strength, and in addition, strengths of 1 and 10% were tried for aluminum etchant, and a strength of 1% was tried for aluminum chloride.

With 5 V reverse bias, boric acid, 1% aluminum chloride, and 1% aluminum etchant produced negligible etching of the cell's aluminum back contact; aluminum chloride and chromium chloride caused vigorous etching, starting from the aluminum isolation scribe; 5% chlorides of ammonia, nickel, sodium and tin also caused vigorous etching of the aluminum.

Some electrolytes, notably boric acid and aluminum chloride have the peculiar property of removing cell aluminum wherever slight planar imperfections occur, when reverse bias is applied. A slight scratch placed on the aluminum will thus be etched within a fraction of a second upon application of 5 V reverse bias.

Another important aspect of the technique is the choice of material with which to make electrical contact to the cell. The most promising material is aluminum. Other materials tend to cause etching of the aluminum back contact of the cell, presumably because of the difference between the electrochemical potentials of these materials and that of aluminum.

Effective defect removal occurs using 1% solutions of either aluminum etchant or aluminum chloride. In some plates, most, but not all defects are removed, and minor damage is done to the panel. Some of these difficult-to-remove defects were made visible by the techniques of the labor-intensive method previously described, and were found to be unremovable by any known technique (without causing serious damage to the panel).

Thus, results obtained so far concerning large area shunt removal are encouraging, and further work needs to be done on these techniques.

4.4 Fused Interconnect

It is desirable to develop a technique that permits fusion of the back metal contact to the front transparent conductive oxide (SnO_2) by means of a laser. In this way, the back contact can be applied to the silicon immediately after silicon deposition, and the laser processing steps can be reduced by one.

Initial work in this area involved experimentation wherein a 0.53μm laser beam was incident on the glass side of the panel, which was metallized with aluminum. With this technique, we achieved scribes 100μm wide, having contact resistances in the range 5-10 ohm-cm. The resistances were, however, unstable, and showed blistering of the aluminum and crystallization of the silicon. The contact resistance here is defined as the series resistance caused by a 1 cm interconnect (scribe) length.

Later experiments involved laser beams incident on the aluminum side. For these experiments, the aluminum is sometimes first coated with approximately 150Å of titanium, in order to better absorb the incident energy. Laser beams with wavelengths 0.53 and 1.06μm were used. Scribes using this latter technique were made with a survey of laser parameters, varying beam size, power, pulse rate, and scan speed. Scribes were then evaluated for stability by annealing at 100°C for one hour.

The best scribes obtained have contact resistances around 1 ohm-cm, and these contain the Ti overcoating. Scribes without the Ti overcoating produced contact resistances in the range 1.3 - 1.5 ohm-cm. In order to limit power losses in the scribe contact to 2% of maximum cell power, the scribe contact resistance should be in the neighborhood of 1 ohm-cm. However, some of the scribes reported are sensitive to annealing, which may cause the contact resistance to either increase or decrease. Thus, more effort must be placed on achieving greater stability of these scribes. We have also set up equipment to permit simultaneous, though out of phase, irradiation with 0.53μm and 1.06μm beams.

4.5 Long Term Outdoor Testing

In Fig. 11, we present data taken by SERI on a Chronar 1 x 1 ft.^{2} glass-glass encapsulated tandem submodule. This submodule is being monitored at SERI's outdoor testing facility in Golden, Colorado. Its initial aperture area efficiency was 5.7%. The long-term performance is quite acceptable, showing only an 11% loss in efficiency after 145 days of outdoor exposure, with indications that light-induced effects are leveling off. The top and bottom stack i-layer thicknesses were 0.073 and 0.44 μm, respectively. The efficiency loss of single-junction submodules in the field appears to be about 1.5 times that experienced by tandem junction submodules.

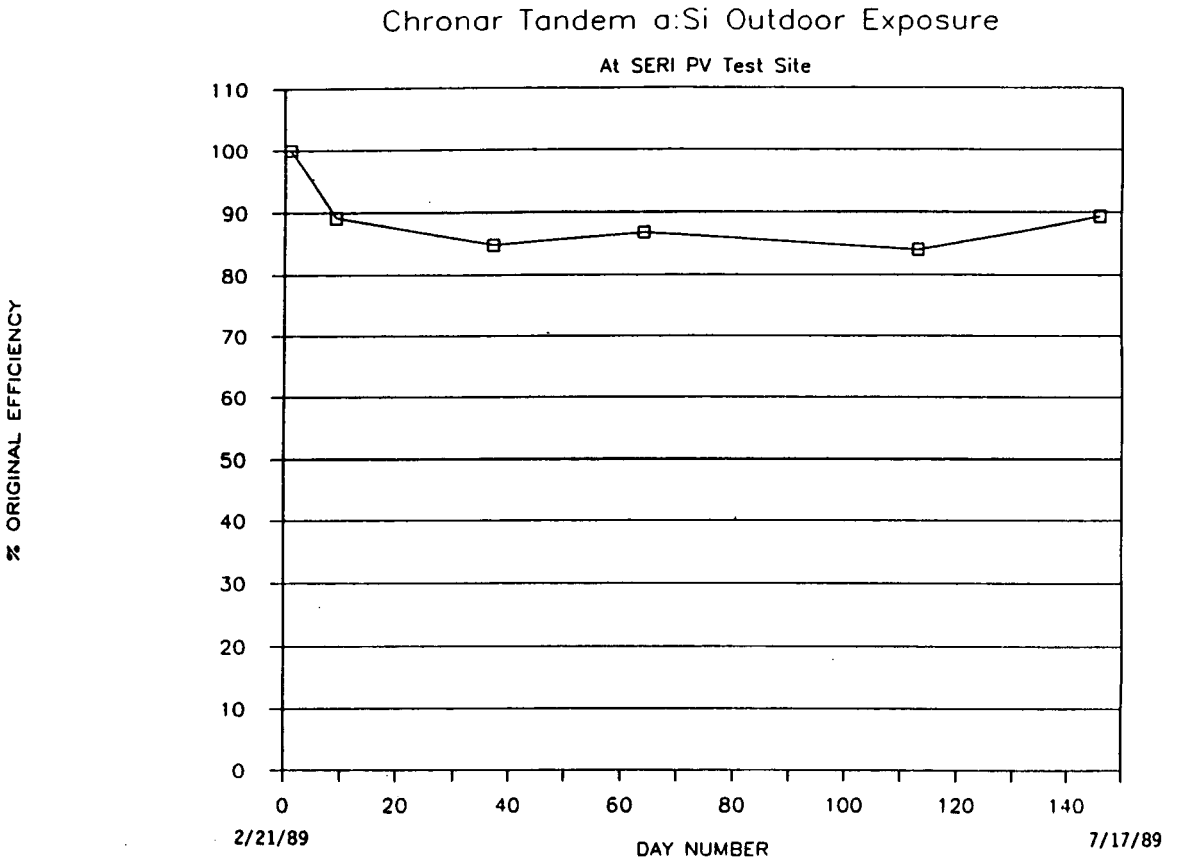

Fig. 11 Long term outdoor performance of a 1 ft.sq. glass-glass encapsulated tandem submodule. (Chronar panel DL321; data courtesy of L. Mrig, SERI).

REFERENCES

1. Annual Technical Progress Report for Phase I (March 16, 1987 - March 15, 1988) Subcontract ZB-7-06003-1.

2. H. Tanaka, K. Miyachi, Y. Ohashi, and N. Fukuda, Phil. Mag. B60 (1989) 101.

3. Annual Technical Progress Report for Phase II (March 16, 1988 - March 15, 1989) Subcontract ZB-7-06003-1.

4. A.E. Delahoy, Recent Developments in Amorphous Silicon Photovoltaic Research and Manufacturing at Chronar Corporation. SERI PV AR&D 9th Review Meeting, Lakewood, CO, May 1989, and to be published in Solar Cells.

5. J. Kalina, H. Schade, A.E. Delahoy, Correlation between Fill factors of Amorphous Silicon Solar Cells and their I-layer Densities of States as Determined by DLTS. SERI PV AR&D 9th. Review Meeting, Lakewood, CO, May 1989, and to be published in Solar Cells.

6. J. Kalina, A.E. Delahoy, and H. Schade, Correlation between Fill Factors in P-I-N Solar Cells and Densities of State in Their I-layers, Proc. 9th European Photovoltaic Solar Energy Conf. (W. Palz, G.T. Wrixon, P. Helm, Eds.) Kluwer, Dordrecht, 1989, p. 84.

7. A.E. Delahoy, J. Kalina, C. Kothandaraman, and T. Tonon, Advanced Technology Amorphous Silicon Photovoltaic Modules, Proc. 9th European Photovoltiac Solar Energy Conf. (W. Palz, G.T. Wrixon, P. Helms, Eds.) Kluwer, Dordrecht, 1989, p. 599.

8. W.A. Nevin, H. Yamagishi, and Y. Tawada, Appl. Phys. Lett. 54 (1989) 1226.

9. F.B. Ellis, Jr., J. Houghton, Chemical Vapor Deposition of Silicon Dioxide Barrier Layers for Conductivity Enhancement of Tin Oxide Films. J. Mat. Res. 4 (1989) 863.

10. T. Minami, H. Nanto, S. Takata, Thin Solid Films 124 (1985) 43.

11. T. Minami, H. Nanto, S. Takata, Jap. J. Appl. Phys. 251 (1986) L 776.

12. R.E.I. Schropp, A. Madan, J. Appl. Phys. 66 (1989) 2027.

Document Control Page	1. SERI Report No. SERI/TP-211-3667	2. NTIS Accession No. DE90000320	3. Recipient's Accession No.

4. Title and Subtitle
Research on Amorphous Silicon-Based Thin Film Photovoltaic Devices Task B: Research on Stable High-Efficiency Large Area, Amorphous Silicon Based Submodules

5. Publication Date
March 1990

6.

7. Author(s)
A.E. Delahoy, Principal Investigator

8. Performing Organization Rept. No.

9. Performing Organization Name and Address
Chronar Corporation
P.O. Box 177
Princeton, New Jersey 08542

10. Project/Task/Work Unit No.

11. Contract (C) or Grant (G) No.
(C) ZB-7-06003-1
(G)

12. Sponsoring Organization Name and Address
Solar Energy Research Institute
1617 Cole Boulevard
Golden, Colorado 80401-3393

13. Type of Report & Period Covered
Technical Report

14. 3/16/89 - 11/30/89

15. Supplementary Notes
SERI Technical Monitor: W. Luft, (303) 231-1823

16. Abstract (Limit: 200 words)

17. Document Analysis
a. Descriptors Photovoltaics ; thin films ; efficiency ; semiconductor materials

b. Identifiers/Open-Ended Terms

c. UC Categories 271

18. Availability Statement
National Technical Information Service
U.S. Department of Commerce
5285 Port Royal Road
Springfield, Virginia 22161

19. No. of Pages
48

20. Price
A03

Form No. 0069 (3-25-82)